PNAS RESEARCH ARTICLE | GENETICS

Germline *BARD1* variants predispose to mesothelioma by impairing DNA repair and calcium signaling

Flavia Novelli[a], Yoshie Yoshikawa[b], Veronica Angela Maria Vitto[c], Lorenzo Modesti[c], Michael Minaai[a], Sandra Pastorino[a], Mitsuru Emi[a], Jin-Hee Kim[a], Franz Kricek[d], Fang Bai[e], José N. Onuchic[f], Angela Bononi[a], Joelle S. Suarez[a], Mika Tanji[a], Cristina Favaron[a], Alicia A. Zolondick[a,g], Ronghui Xu[a], Yasutaka Takanishi[a], Zhanwei Wang[a], Greg Sakamoto[a], Giovanni Gaudino[a], Joseph Grzymski[h], Federica Grosso[i], David S. Schrump[j], Harvey I. Pass[k], Lilit Atanesyan[l], Jan Smout[l], Suvi Savola[l], Kavita Y. Sarin[m], Hassan Abolhassani[n], Lennart Hammarström[n], Qiang Pan-Hammarström[n], Carlotta Giorgi[c], Paolo Pinton[c], Haining Yang[a], and Michele Carbone[a,1]

Affiliations are included on p. 11.

Edited by Peter Vogt, Scripps Research Institute Department of Molecular Medicine, La Jolla, CA; received March 13, 2024; accepted June 12, 2024

We report that ~1.8% of all mesothelioma patients and 4.9% of those younger than 55, carry rare germline variants of the BRCA1 associated RING domain 1 (*BARD1*) gene that were predicted to be damaging by computational analyses. We conducted functional assays, essential for accurate interpretation of missense variants, in primary fibroblasts that we established in tissue culture from a patient carrying the heterozygous *BARD1*^{V523A} mutation. We found that these cells had genomic instability, reduced DNA repair, and impaired apoptosis. Investigating the underlying signaling pathways, we found that BARD1 forms a trimeric protein complex with p53 and SERCA2 that regulates calcium signaling and apoptosis. We validated these findings in *BARD1*-silenced primary human mesothelial cells exposed to asbestos. Our study elucidated mechanisms of *BARD1* activity and revealed that heterozygous germline *BARD1* mutations favor the development of mesothelioma and increase the susceptibility to asbestos carcinogenesis. These mesotheliomas are significantly less aggressive compared to mesotheliomas in asbestos workers.

genetics | carcinogenesis | mesothelioma | gene × environment | cancer prevention

Significance

There has been an unexplained increase of mesothelioma in younger patients who have not worked in the asbestos industry. We report that inherited germline mutations of *BARD1* cause some mesotheliomas in young patients. They experience significantly prolonged survival up to 20+ y and they require tailored screening and therapeutic approaches.

Cancer for the most part is a disease of old age, however, in recent years there has been an unexplained increase of cancer diagnoses among young patients. Various hypotheses, including exposure to increasing amounts of environmental carcinogens, have been proposed, yet there are no firm data to support these hypotheses (1). Mesothelioma, one of the best examples of a cancer caused by environmental carcinogens, is one of the malignancies that we see with increasing frequency in younger patients (2). This is very difficult to explain because asbestos causes cancer about 30 to 60+ y after initial exposure, thus most asbestos workers developed mesothelioma when they are old (2). Because, asbestos use was banned in the 80 s (2), former asbestos workers are now in their 70 s to 90 s, thus we should see mesothelioma in older not younger patients! (3)

In previous studies, we found that heterozygous germline mutations in the *BAP1* gene cause the BAP1 Cancer Syndrome, characterized by a high incidence of mesothelioma (4–9). We found that *BAP1*-linked mesotheliomas had a distinct clinical presentation: These patients very rarely had evidence of asbestos exposure, the median age of onset was 54 y old, several of them were in their 20 s and 30 s, the male to female and the pleural to peritoneal mesothelioma ratios were 1:1, compared to about 7:1 in mesotheliomas developing in asbestos workers (8, 10–12). Intriguingly, mesotheliomas developing in carriers of germline *BAP1* mutations had a median survival of 5 ~ 7 y and some were apparently cured as they survived mesothelioma for >20 y (8, 10–16). In contrast, mesotheliomas developing in asbestos workers have a median survival of ~1 y, are resistant to therapy, and are uniformly fatal (14). These differences point to different mechanisms underlying the pathogenesis of these malignancies. In additional targeted next-generation sequence studies we, and others, found that ~8 to 16% of mesotheliomas developed in carriers of germline *BAP1* mutations—the most frequent mutations—and, occasionally, in the contest of other tumor predisposition syndromes (8, 10–16). We also found some mesotheliomas developing in younger patients and associated with prolonged survival that did not contain mutations of any of the genes tested, which included those known to predispose to cancer (11). We suspected that additional genes, not included in our testing panel (11) might cause or predispose to less aggressive mesotheliomas in younger patients. It is important to identify carriers of germline mutations that predispose to cancer because screening of these individuals and of their affected family members for early cancer detection can be life-saving. Also, when diagnosed with cancer, these patients

Author contributions: F.N., V.A.M.V., L.M., J.-H.K., F.K., J.S.S., G.G., C.G., P.P., H.Y., and M.C. designed research; F.N., Y.Y., V.A.M.V., L.M., J.-H.K., F.K., A.B., J.S.S., C.F., A.A.Z., L.A., J.S., S.S., and H.A. performed research; Y.Y., M.M., S.P., M.E., F.K., F.B., J.N.O., M.T., R.X., Y.T., Z.W., G.S., J.G., F.G., D.S.S., H.I.P., L.A., J.S., S.S., K.Y.S., H.A., L.H., Q.P.-H., C.G., and P.P. contributed new reagents/analytic tools; F.N., Y.Y., V.A.M.V., L.M., M.M., S.P., M.E., J.-H.K., F.K., A.B., M.T., C.F., A.A.Z., Y.T., J.G., L.A., J.S., S.S., H.A., L.H., Q.P.-H., C.G., P.P., H.Y., and M.C. analyzed data; M.C. supervision; and F.N. and M.C. wrote the paper.

Competing interest statement: M.C. has a patent issued for "Methods for Diagnosing a Predisposition to Develop Cancer." M.C. and H.Y. have a patent issued for "Using Anti-HMGB1 Monoclonal Antibody or other HMGB1 Antibodies as a Novel Mesothelioma Therapeutic Strategy", and a patent issued for "HMGB1 As a Biomarker for Asbestos Exposure and Mesothelioma Early Detection." M.C. is a board-certified pathologist who provides consultation for pleural pathology, including medical-legal.

This article is a PNAS Direct Submission.

[1]To whom correspondence may be addressed. Email: mcarbone@cc.hawaii.edu.

This article contains supporting information online at https://www.pnas.org/lookup/suppl/doi:10.1073/pnas.2405231121/-/DCSupplemental.

Published July 11, 2024.

have a better prognosis and may respond to specific target therapies (8, 13, 17, 18).

Our hypothesis was that mutations in genes whose disrupted functions would lead to alteration in signaling pathways similar to those caused by *BAP1* mutations might also cause mesothelioma and that these mesotheliomas would be less aggressive. *BARD1* appeared to be a possible candidate because although *BAP1* stands for "BRCA1-associated-protein-1" (19) a subsequent study proposed that BAP1 does not bind BRCA1, rather it binds BARD1 preventing its binding to BRCA1 (20). The BRCA1/BARD1 complex has E3 ligase activity and modulates DNA repair by homologous recombination. Therefore, *BARD1* similarly to *BRCA1* and *BAP1*, modulates DNA repair (21–23). In the cytoplasm BARD1 competes with Mouse Double Minute 2 homolog (MDM2) to bind TP53 (24–26). *BARD1* inactivating mutations allow MDM2 to bind p53, which is therefore ubiquitylated and degraded, impairing p53-induced apoptosis. Recent findings revealed a negative genetic interaction between BLM loss and BARD1 deficiency that leads to chromosomal breakage, micronucleation, and cell death (27). Some germline *BARD1* mutations and large deletions have recently been linked to breast and ovarian cancer and possibly to neuroblastoma (28–32). The possible causative association of germline *BARD1* mutations with other human cancers remains speculative (33). Accordingly, most germline *BARD1* mutations are classified in ClinVar either as benign or as variant of unknown significance, largely because of the lack of integrated clinical and mechanistic evidence required to establish cause-effect relationships. We reasoned that if BAP1 interacts with BARD1 to modulate homologous recombination and possibly other cellular pathways, germline *BARD1* mutations might also predispose to mesothelioma, and that these patients might have a better prognosis, similar to carriers of germline *BAP1* mutations.

Results

Identification of Germline Mutations in the *BARD1* Gene of Mesothelioma Patients. We searched The Cancer Genome Atlas (TCGA) mesothelioma datasets for genetic determinants of cancer survival (tcga-survival.com) and found 37 mesothelioma patients with low BARD1 expression. These patients had a significantly increased median survival compared to patients with high BARD1 expression (P = 0.009679, Fig. 1*A*). We verified and confirmed that BAP1 coprecipitates with BARD1 and not with BRCA1 (*SI Appendix*, Fig. S1*A*).

We investigated a cohort of 61 patients who developed mesothelioma at young age (55< y old) and who had no evidence of asbestos exposure. Their DNA samples were sequenced and analyzed for the presence of *BARD1* mutations using comprehensive techniques, including Whole Exome Sequencing (WES) to identify Single Nucleotide Variants—results verified by Sanger sequencing—and digital multiplex ligation-dependent probe amplification (digital-MLPA) to identify copy number variations ranging from whole chromosomes to single exons (34, 35). We used the Combined Annotation Depletion (CADD, version 1.6) score to rate the potential deleteriousness of the identified *BARD1* variants. CADD utilizes machine learning on a variety of genomic features derived from surrounding sequence context, gene model annotations, evolutionary constraints, and functional predictions (36). The Minor Allele Frequency (MAF) for the variations found in the research cohort was defined using the Genome Aggregation Database (gnomAD, version 2) (37). Finally, we used the MutationSignificance Cutoff (MSC), a gene-specific score to identify the lowest expected clinical-biological relevant CADD score value (38). 27/61 (44.2%) carried pathogenic *BAP1* variants with a CADD score ≥20 (MSC = 18.4). Our previous results showed that all *BAP1* mutations with a CADD score >18 and with a MAF < 0.01-i.e., rare variants–were pathogenic and could be causally linked to mesothelioma (11, 39, 40). Single patients carried pathogenic rare variants in tumor suppressor genes, including *BRCA1*, *BRCA2*, *TP53*, etc., that are well known to cause other tumor predisposition syndromes. Three of 61 mesothelioma patients (4.9%) carried rare, MAF < 0.01, heterozygous germline *BARD1* variants with CADD scores >20 (MSC = 14.2); all of them had a significantly prolonged survival (*SI Appendix*, Tables S1 and S2). Among these three mesothelioma patients, two had different missense *BARD1* variants and one carried a *BARD1* deletion (Fig. 1 *B* and *C* and *SI Appendix*, Fig. S1 *B–D* and Tables S1 and S2).

About 90% of mesotheliomas contain either or both *BAP1* and *CDKN2A* somatic (acquired) biallelic inactivating mutations—*CDKN2A* codes for p14 and p16. Inactivation of these genes is considered the main driver of sporadic -not genetically related- mesothelioma (41–43). The mesothelioma biopsy from the patient carrying *BARD1*^{V523A} was available to us. Immunohistochemistry (IHC) showed that BAP1 expression was retained in the *BARD1*^{V523A} mesothelioma cells, evidence of wild-type *BAP1* (41, 44). Fluorescence in situ hybridization was negative for homozygous deletion of the *CDKN2A* (9p21). These findings were supported by IHC that showed p16 nuclear expression in the mesothelioma cells (*SI Appendix*, Fig. S2 *A* and *B*). In summary, neither *BAP1* nor *CDKN2A* inactivation contributed to mesothelioma, at least in one of these three patients.

We considered whether the 2 *BARD1* mutations and the *BARD1* deletion described above might be causally linked to mesothelioma because of their high in silico pathogenicity prediction scores, their low frequency in the human population, the early onset of these mesotheliomas and the unusually significant prolonged survival of these three patients. *BARD1* mutations have not been linked to mesothelioma to date. The two missense *BARD1* mutations (Val523Ala, Arg43Ser) are listed on ClinVar with "conflicting interpretation" for the Val53Ala and "uncertain significance" for the Arg43Ser; the *BARD1* deletion (7–11) is not in ClinVar. In summary, the ClinVar archive did not help us judge their possible pathogenicity.

Distinguishing pathogenic from harmless variants in the absence of clinical data and large family pedigrees showing cosegregation—which are rarely available—is challenging (45). There is a general agreement that functional assays are essential for accurate interpretation of missense variants and that current prediction tools, including CADD, should be used with caution (46). The *BARD1*^{V523A} variant had been tested with unclear results in a study that used an assay for homology-directed DNA repair in which 76 *BARD1* variants were screened. In that assay, the *BARD1*^{V523A} mutation showed a reduced nonsignificant difference in DNA repair (47).

To assess the biologic consequences of mutated *BARD1* resulting in reduced BARD1 protein levels we established fibroblast cultures from the *BARD1*^{V523A} variant carrier (FM-26), a living patient with the longest mesothelioma survival (>23 y). This patient had diffuse peritoneal mesothelioma with widespread multiple tumor nodules throughout the abdominal cavity, biopsies of her tumor demonstrated tumor cell invasion (Fig. 1*D* and *SI Appendix*, Fig S1*B*). Visible tumor nodules were ablated and she was treated with chemotherapy, expected survival was ~12 mo: 23 years later she is alive and well.

Studying the primary cells of this patient without any laboratory manipulation we ensured that the results were specific for the *BARD1*^{V523A} and were not affected by technical manipulation. To validate the general relevance of the results studying this particular variant, we down-regulated *BARD1* in primary benign Human Mesothelial cells (HM) that we established in tissue culture from pleural fluids of patients with nonmalignant conditions. In the

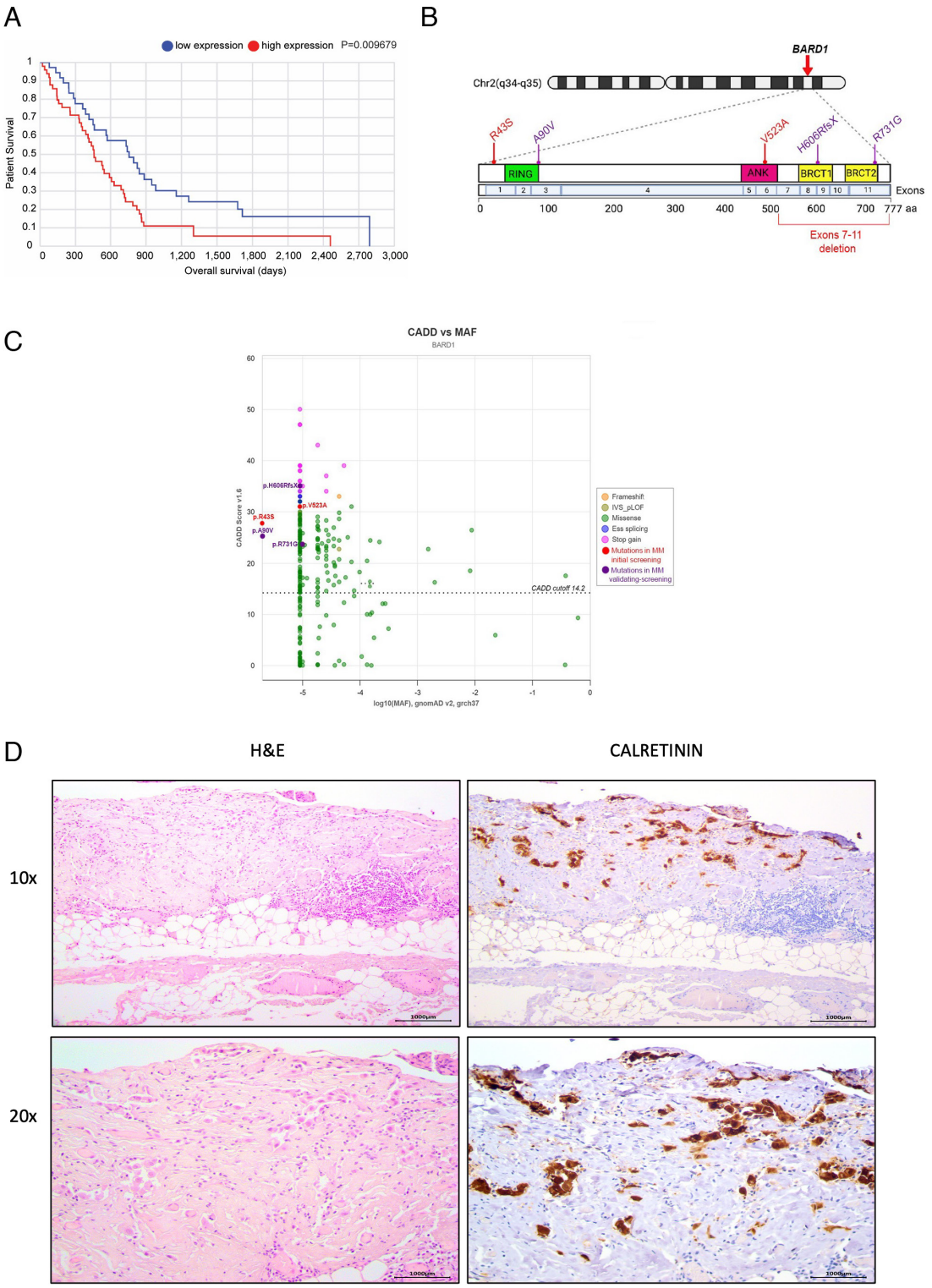

Fig. 1. Germline heterozygous *BARD1* mutations found in different individuals with history of mesothelioma. (*A*) Survival plot showing percentage of survival vs. time in low and high BARD1 expression related mesothelioma cases analyzed by TGCA database. (*B*) Schematic representation of the *BARD1* gene and protein. Localization of *BARD1* to chromosome 2 (red arrow) and diagram of the full-length BARD1 protein (777 aa) showing the six likely pathogenic germline *BARD1* mutations we identified in six mesothelioma patients (*SI Appendix*, Tables S1 and S2): three detected in the initial screening (marked in red) and three detected in the validating screening (marked in violet). BARD1 domains are shown: RING domain (green), ANK (pink), BRCT domains (yellow). Exons and amino acids are numbered in gray and black. (*C*) Combined Annotation Dependent Depletion (CADD) score vs. Minor Allele Frequency (MAF) plot for *BARD1* variants. The horizontal axis shows MAF based on gnomAD (version 2) from the Caucasian population. The vertical axis presents the scores of CADD (version 1.6) predicting the pathogenicity of these variants. Five of the six *BARD1* mutations found in our patients, are highlighted in red or violet. The 6th mutation consisted of a large *BARD1* deletion spanning exons 7 to 11 and shown in Fig. 1*B*. Because of the large deletions it is not possible to generate a CADD score. The gene-specific Mutation Significant Cutoff (MSC) for CADD score for *BARD1* is 14.2, as indicated by the dotted line. (*D*) Hematoxylin and Eosin (H&E) and CALRETININ immunostaining of the mesothelioma tumor tissue biopsy from *BARD1*^{V523A} carrier (female). Photomicrograph at 100× and 200×. (Scale bar: 1,000 μm.)

assays described below we considered that mesothelial cells are very susceptible to asbestos-induced DNA damage, cell death, and transformation (measured as foci formation) (48). Fibroblasts, instead, are not susceptible to asbestos toxicity; however, they are susceptible to radiation and H_2O_2-induced DNA damage and cell death (48).

Germline *BARD1*^{V523A} Heterozygous Mutation and Reduced BARD1 Levels Increase Genome Instability and DNA Damage In Vitro. The ability of BARD1 to modulate DNA repair by homologous recombination has been ascribed to its nuclear localization. Subcellular fractionation of primary *BARD1*^{WT} and *BARD1*^{V523A} fibroblasts revealed that the amount of BARD1 protein was specifically reduced in the nuclear fraction of *BARD1*^{V523A} fibroblasts compared to *BARD1* wild-type (*BARD1*^{WT}) control fibroblasts from a donor matched by sex and age (Fig. 2*A*). These findings were supported by immunofluorescence (IF) showing that BARD1 protein levels were significantly reduced in the nucleus of *BARD1*^{V523A} fibroblasts (*SI Appendix*, Fig. S3 *A* and *B*). Together these findings suggested a reduced BARD1 nuclear activity.

We tested the response of *BARD1*^{V523A} to DNA damage by measuring the number of micronuclei in primary human *BARD1*^{WT} and *BARD1*^{V523A} fibroblasts exposed to 1GY of ionizing radiation

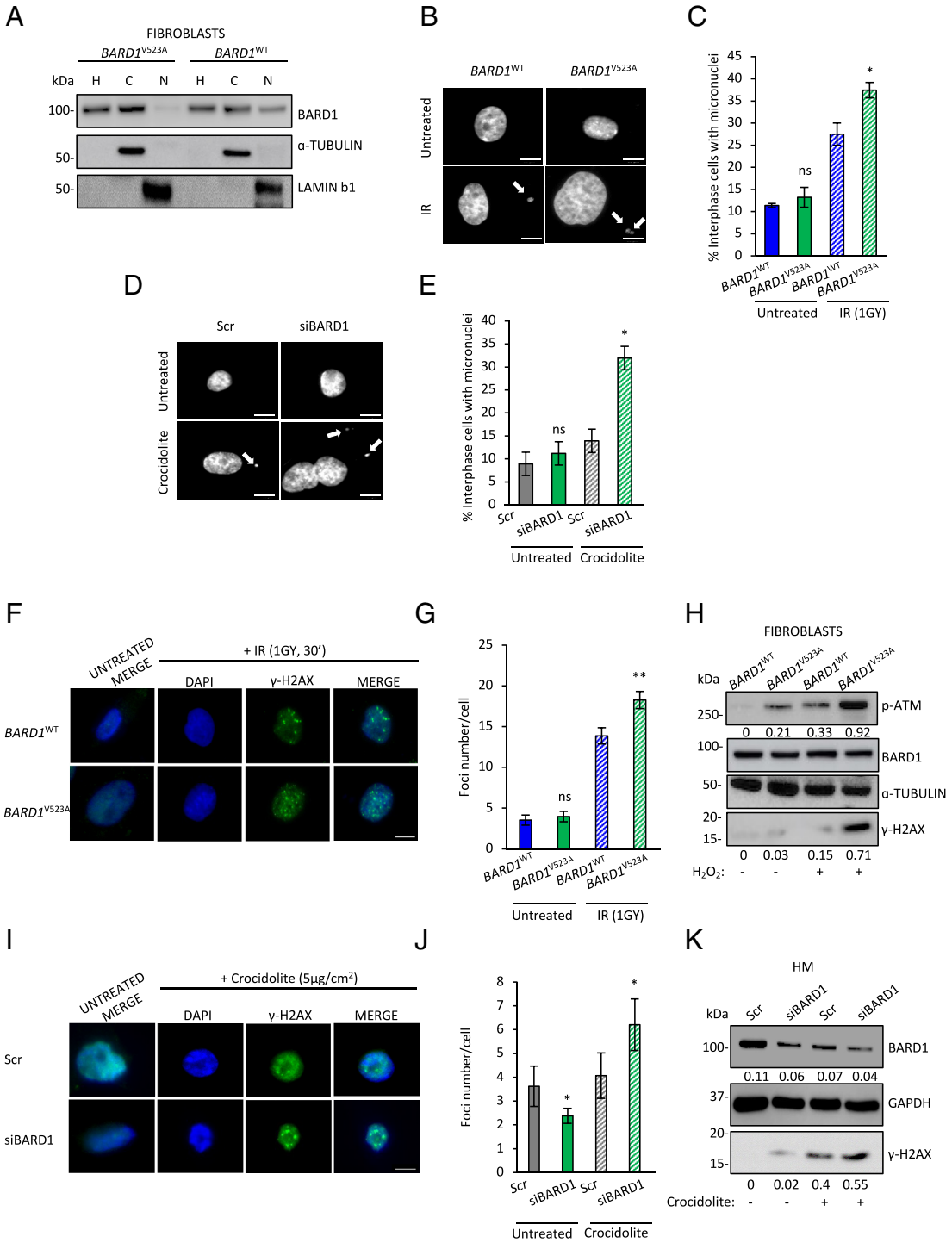

Fig. 2. Effects of *BARD1*^{V523A} mutation and of reduced BARD1 levels in DNA damage response. (*A*) Nuclear-cytoplasmic fractionation of *BARD1*^{WT} and *BARD1*^{V523A} fibroblasts. Reduced nuclear BARD1 localization was detected in *BARD1*^{V523A} fibroblasts compared to *BARD1*^{WT} cells. Abbreviations: H, Homogenate; C, Cytoplasm; N, Nucleus. (*B–E*) Chromosomal instability was determined as micronuclei frequency at interphase. (*B*) Primary human *BARD1*^{WT} and *BARD1*^{V523A} fibroblasts were treated with 1GY ionizing radiation (IR) for 5 min in PBS or left untreated (PBS); 48 h later, the number of micronuclei (indicated by white arrows) was determined by DAPI staining. (Scale bars: 10 μm.) (*C*) Percentage of interphase cells with micronuclei in ≥140 cells counted per treatment from n = 2 *BARD1*^{WT} and n = 2 *BARD1*^{V523A} mutant; data shown as one representative experiment. *P* values are calculated by unpaired two-tailed Student's *t* tests (**P* < 0.05). (*D*) Primary HM cells were transfected with a pool of siRNAs for *BARD1* gene (siBARD1) or a control siRNA (Scr) and then treated with 5 μg/cm^2 crocidolite for 24 h or left untreated (PBS); 48 h later, the number of micronuclei (indicated by white arrows) was determined by DAPI staining. (Scale bars: 10 μm.) (*E*) Percentage of interphase cells with micronuclei in ≥140 cells counted per treatment from n = 3 independent experiments; data are shown as mean ± SD. *P* values are calculated by unpaired two-tailed Student's *t* tests (**P* < 0.05). (*F* and *G*) γ-H2AX foci formation in *BARD1*^{WT} and *BARD1*^{V523A} fibroblasts upon DNA damage. (*F*) *BARD1*^{WT} and *BARD1*^{V523A} fibroblasts were treated with 1GY IR for 5 min in PBS or left untreated (PBS), followed by a recovery of 30 min and stained for endogenous γ-H2AX. (Scale bars: 10 μm.) (*G*) Number of γ-H2AX foci in 30 cells counted per each group. *P* values are calculated by unpaired two-tailed Student's *t* tests (***P* < 0.01). (*H*) Western blot comparing γ-H2AX protein levels in *BARD1*^{WT} and *BARD1*^{V523A} fibroblasts after the treatment with 100 μM H_2O_2 for 24 h (+) or left untreated (−). (*I* and *J*) γ-H2AX foci formation in HM cells silenced for *BARD1* gene. (*I*) Primary HM cells were transfected with a pool of siRNAs for *BARD1* gene (siBARD1) or a control siRNA (Scr) and then treated with 5 μg/cm^2 crocidolite for 24 h or left untreated (PBS); 24 h later, the γ-H2AX foci number in each cell was counted. At least 35 cells were included per each group. (Scale bars: 10 μm.) (*J*) Number of γ-H2AX foci in 35 cells counted per each group. *P* values are calculated by unpaired two-tailed Student's *t* tests (**P* < 0.05). (*K*) Western blot comparing γ-H2AX protein levels in HM cells silenced for BARD1. DNA damage in HM cells silenced for *BARD1* gene and exposed to 5 μg/cm^2 crocidolite for 24 h (+). Decimals: BARD1/GAPDH, γ-H2AX/GAPDH, p-ATM/α-TUBULIN, γ-H2AX/α-TUBULIN.

(IR). We found a significant increase in the number of micronuclei in *BARD1*^{V523A} fibroblasts ($P < 0.05$) (Fig. 2 *B* and *C*). We validated these findings in primary HM exposed to crocidolite, the most carcinogenic among asbestos fibers (49). BARD1 was silenced using a pool of four individual siRNAs targeting *BARD1* (siBARD1); a nonspecific siRNA (scramble) was used as control. Micronuclei occurred at a significantly higher frequency in *BARD1*-silenced HM exposed to asbestos compared to control (Scr) (*$P < 0.05$) (Fig. 2 *D* and *E*).

Phosphorylation of histone H2AX at serine 139 (γ-H2AX) is an early cellular response to DNA double-strand breaks. Upon DNA damage, γ-H2AX is localized to discrete nuclear foci that can be used as indicator of DNA damage (50). *BARD1*^{V523A} mutant fibroblasts showed a significant increase in the γ-H2AX foci upon exposure to 1GY of IR compared to *BARD1*^{WT} fibroblasts (Fig. 2 *F* and *G*). In parallel experiments, treatment of primary *BARD1*^{WT} and *BARD1*^{V523A} fibroblasts with H_2O_2 for 24 h to induce DNA damage led to an increase in the phosphorylation of H2AX and ATM proteins in human *BARD1*^{V523A} fibroblasts (Fig. 2*H*). In parallel, we detected a significant increase in the number of γ-H2AX foci after crocidolite exposure (Fig. 2 *I* and *J*), as well as an increased expression of γ-H2AX protein in *BARD1*-silenced HM cells compared to controls (Fig. 2*K*). Kinetics analyses showed a prolonged phosphorylation of H2AX indicating that DNA repair was delayed in *BARD1*^{V523A} compared to the *BARD1*^{WT} fibroblasts (*SI Appendix*, Fig. S3*C*).

Reactive oxygen species (ROS) induce DNA damage and may contribute to malignant transformation (51). We observed a significantly higher intracellular ROS production in *BARD1*^{V523A} fibroblasts that was further enhanced upon exposure to 1GY of IR (*SI Appendix*, Fig. S3*D*). Investigating this finding, we found that *BARD1*^{V523A} mutant fibroblasts produce more mitochondrial ROS compared to *BARD1*^{WT} cells (*SI Appendix*, Fig. S3*E*). Downregulation of BARD1 in primary HM exposed to asbestos resulted in a significant increase of intracellular ROS production, as well (*SI Appendix*, Fig. S3*F*).

In summary, we found that primary *BARD1*^{V523A} fibroblasts show reduced amounts of nuclear BARD1 protein, resulting in increased genome instability, delayed DNA repair, and they produce higher amounts of mutagenic ROS compared to primary fibroblasts containing *BARD1*^{WT}. These findings were reproduced in primary HM cells exposed to asbestos in which we down-regulated BARD1 expression.

***BARD1*^{V523A} Destabilizes p53 Impairing Ca^{2+} Homeostasis and Apoptosis.** The *BARD1*^{V523A} mutation is in the ANKYRIN (ANK) domain that binds and stabilizes p53 (26, 52). Coimmunoprecipitation assays (Co-IP) revealed reduced BARD1–p53 interaction in primary *BARD1*^{V523A} fibroblasts compared to both *BARD1*^{WT} and to *BAP1*$^{+/-}$ primary fibroblasts—controls—(Fig. 3*A*). *BARD1*^{WT} and *BARD1*^{V523A} fibroblasts were treated with H_2O_2 to induce cell death: We found reduced CLEAVED CASPASE-3 and reduced p53 levels in *BARD1*^{V523A} fibroblasts compared to *BARD1*^{WT} control cells (Fig. 3*B*). In parallel, in *BARD1*-silenced HM exposed to asbestos, we detected lower amounts of cleaved caspase-3 compared to controls (Fig. 3 *C* and *D*). Moreover, p53 levels were reduced in *BARD1*-silenced HM cells (Fig. 3 *C* and *D*). These results suggested that the reduced BARD1–p53 interaction led to decreased p53 protein levels and reduced apoptosis.

We demonstrated that dysregulation of intracellular calcium (Ca^{2+}) homeostasis reduces apoptosis and plays a key role in promoting mesothelioma in carriers of germline *BAP1* mutations because these mutations impair IP3R3 the Ca^{2+} channel that releases Ca^{2+} from the endoplasmic reticulum (ER) into the cytoplasm/mitochondria (48). Also p53, although through different mechanisms, modulates Ca^{2+} and apoptosis by 1) transcriptional activation of TRPC6, a Ca^{2+} channel located on the cell membrane that controls cellular Ca^{2+} uptake, and 2) binding to and activating SERCA, the Ca^{2+} channel that regulates the uptake of Ca^{2+} into the ER (54–56). We hypothesized that BARD1 might also modulate Ca^{2+} intracellular concentrations and apoptosis by stabilizing p53. Thus, we tested the hypothesis that *BARD1* mutations might reduce ER, cytosolic, and mitochondrial Ca^{2+} concentrations and thus favor malignant transformation by impairing intrinsic apoptosis.

We measured Ca^{2+} concentrations in *BARD1*^{WT} and *BARD1*^{V523A} fibroblasts and in *BARD1*-silenced HM. Upon stimulation with 1 μM Bradykinin (BK) we observed a significant reduction of mitochondrial (Fig. 3 *E–H*) and cytosolic (*SI Appendix*, Fig. S4 *A–E*) Ca^{2+} concentrations in both *BARD1*^{V523A} fibroblasts and in *BARD1*-silenced HM compared to controls. To test whether these Ca^{2+} alterations were specifically caused by the *BARD1* mutation, we transduced *BARD1*^{V523A} fibroblasts with a human BARD1 adenovirus (Ad-BARD1) and we measured mitochondrial Ca^{2+} levels following stimulation with BK. Cells infected with Ad-BARD1 showed significantly increased Ca^{2+} concentrations compared to the control cells infected with a nonspecific GFP adenovirus (Fig. 3 *I* and *J* and *SI Appendix*, Fig. S4*F*). We observed significantly reduced Ca^{2+} concentrations and Ca^{2+} refilling rates in the ER of *BARD1*^{V523A} fibroblasts compared to WT fibroblasts stimulated with $CaCl_2$ (Fig. 3 *K–M*). Using the fluorescent Ca^{2+} indicator Fura-2/AM we detected significantly lower cytosolic Ca^{2+} responses after proapoptotic stimulation with H_2O_2 in *BARD1*^{V523A} fibroblasts compared to the *BARD1*^{WT} fibroblasts (*SI Appendix*, Fig. S4 *G* and *H*) evidence of reduced amounts of Ca^{2+} released from the ER. Next, we investigated possible mechanisms responsible for these effects.

BARD1 Modulates Apoptosis by Stabilizing the TP53–SERCA2 Interaction and TRPC6 Activity. We tested whether BARD1 modulates Ca^{2+} flux in a p53-dependent manner by reducing the activity of TRPC6 and SERCA2 (the dominant isoform in humans) Ca^{2+} pumps. We detected lower TRPC6 protein levels in *BARD1*^{V523A} fibroblasts compared to controls (*SI Appendix*, Fig. S5*A*). Accordingly, qRT-PCR revealed in *BARD1*^{V523A} fibroblasts a significant reduction in the TRPC6 mRNA levels compared to controls (*SI Appendix*, Fig. S5*B*). To test whether the reduced TRPC6 expression was altering Ca^{2+} uptake, we measured the Ca^{2+} concentrations using cytosolic targeted aequorin probes in *BARD1*^{WT} and *BARD1*^{V523A} fibroblasts (*SI Appendix*, Fig. S5 *C* and *D*). We observed significantly reduced cytosolic Ca^{2+} concentrations in *BARD1*^{V523A} fibroblasts compared to WT cells (*SI Appendix*, Fig. S5 *C* and *D*). In parallel experiments, we detected reduced TRPC6 and p53 expression in *BARD1*-silenced HM (*SI Appendix*, Fig. S5*E*).

To investigate whether BARD1 regulates p53–SERCA2 interaction, we coimmunoprecipitated cell lysates from *BARD1*^{WT} and *BARD1*^{V523A} fibroblasts with a p53 antibody and blotted for SERCA2 and p53. The p53–SERCA2 interaction was reduced in *BARD1*^{V523A} compared to *BARD1*^{WT} cells (Fig. 4*A*). A reverse endogenous Co-IP with a SERCA2 antibody produced similar results, even after Adriamycin treatment, a drug that induces p53 overexpression (Fig. 4*B*).

To identify the localization of BARD1, we performed a subcellular fractionation of mesothelioma cells established in culture containing both WT *BARD1* and WT *TP53*. We detected BARD1 expression in the total homogenate, in the cytoplasm, and in the nuclear fraction. We found that BARD1 colocalizes with p53 and SERCA2 in the ER and in the Mitochondria-associated

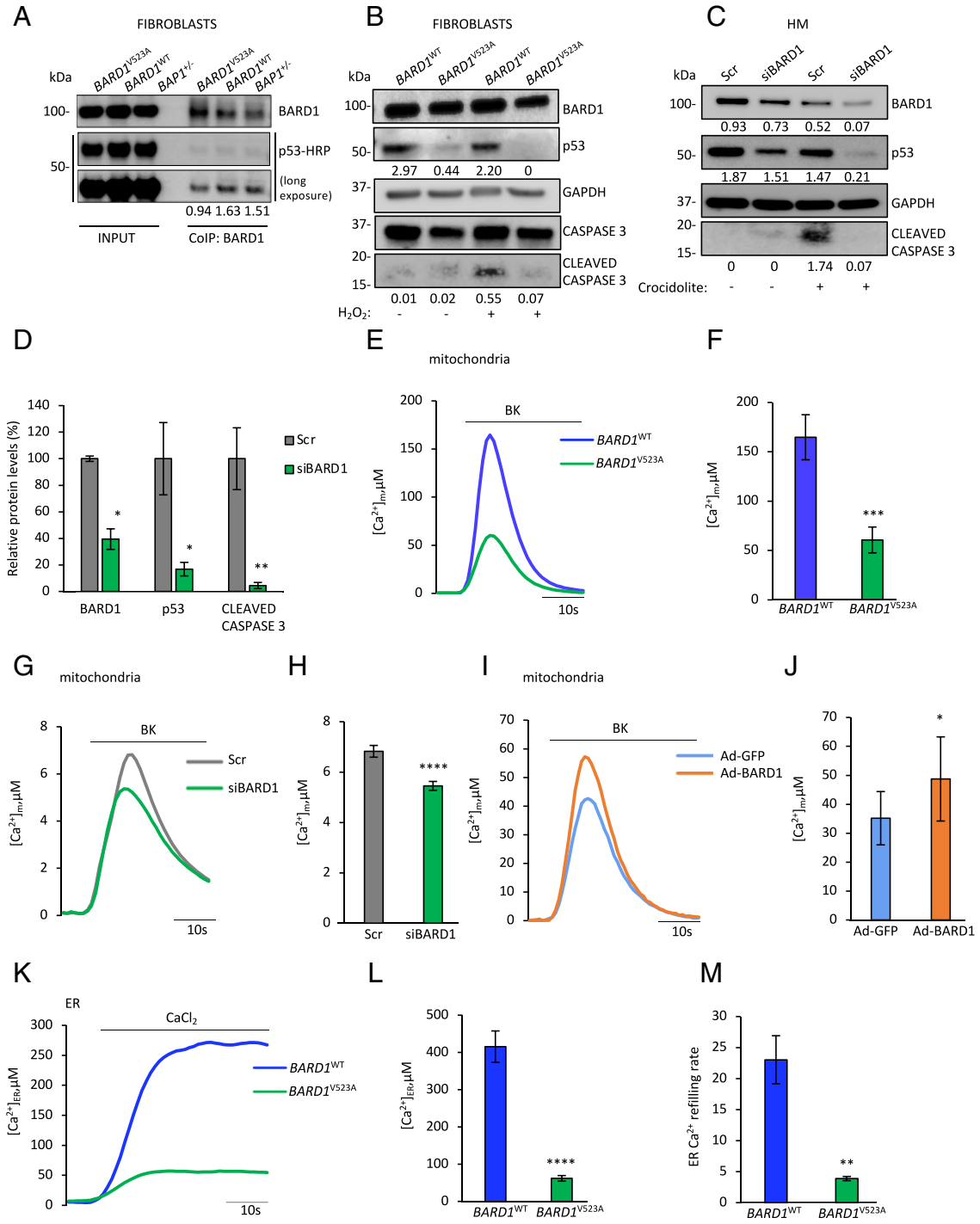

Fig. 3. *BARD1*^{V523A} mutation increases resistance to apoptosis by modulating Ca^{2+} homeostasis. (*A*) Co-IP of endogenous p53 with BARD1 (used as bait) in fibroblast cell cultures from *BARD1*^{WT} individuals or carriers of heterozygous *BARD1*^{V523A} or *BAP1*$^{+/-}$ mutations. Lower amounts of the coprecipitated BARD1–p53 proteins are found in *BARD1*^{V523A} cells. (*B*) Western blot comparing p53 and cleaved caspase-3 levels upon DNA damage. *BARD1*^{WT} and *BARD1*^{V523A} fibroblasts were treated with 100 µM H_2O_2 for 24 h (+) or left untreated (−). P53 and CLEAVED CASPASE-3 levels were reduced in *BARD1*^{V523A} fibroblasts. (*C*) HM cells were transfected with siRNAs for BARD1 (siBARD1) or control siRNA (Scr) and then treated with 5 µg/cm^2 crocidolite for 24 h or left untreated (PBS); Reduced cleaved caspase-3 was detected in *BARD1*-silenced HM after crocidolite treatment. Lower p53 amounts were also found in both untreated or crocidolite-treated *BARD1*-silenced HM. (*D*) Bar graph: BARD1/GAPDH, p53/GAPDH, CLEAVED CASPASE-3/GAPDH densitometry of bands in primary *BARD1*-silenced HM after exposure to 5 µg/cm^2 crocidolite for 24 h, shown as mean ± SD of the n = 4 biological replicates, one displayed in (Fig. 3*C*). (*E–H*) Intracellular mitochondrial Ca^{2+} levels in *BARD1*^{WT} and *BARD1*^{V523A} fibroblasts and in HM transduced with siRNA-CTR or siRNA specific for BARD1. Representative traces of single cells Ca^{2+} measurements using mitochondrial targeted aequorin probe (53) in *BARD1*^{WT} and *BARD1*^{V523A} fibroblasts (*E*) and in HM transduced with siRNA-CTR or siRNA specific for BARD1 (*G*). Reduced intracellular Ca^{2+} in the mitochondria of *BARD1*^{V523A} fibroblasts (*F*) and in *BARD1*-silenced HM (*H*). (*I* and *J*) Mitochondrial Ca^{2+} levels in *BARD1*^{V523A} fibroblasts transduced with Ad-BARD1 or Ad-GFP (Green Fluorescent Protein used as control). (*I*) Representative traces of single cells Ca^{2+} measurements using mitochondrial targeted aequorin probe showing increased mitochondrial Ca^{2+} in *BARD1*^{V523A} fibroblasts upon treatment with 1 µM BK. *BARD1*^{V523A} fibroblasts were transduced with Ad-BARD1(orange line) or Ad-GFP (blue line), used as control. j, Increased intracellular mitochondrial Ca^{2+} levels in *BARD1*^{V523A} fibroblasts upon transduction of Ad-BARD1 compared to the control cells (Ad-GFP). (*K–M*) Ca^{2+} levels in the ER of *BARD1*^{WT} and *BARD1*^{V523A} fibroblasts. (*K*) Representative traces of single cells Ca^{2+} measurements using ER targeted aequorin probe (53) showing decreased ER Ca^{2+} in *BARD1*^{V523A} fibroblasts upon treatment with $CaCl_2$. Significant reduction of total ER Ca^{2+} levels (*L*) and significant reduction of ER Ca^{2+} refilling rate in *BARD1* mutant cells (*M*). Decimals: BARD1/GAPDH, p53/GAPDH, CLEAVED CASPASE-3/CASPASE-3 in *B*; BARD1/GAPDH, p53/GAPDH, CLEAVED CASPASE-3/GAPDH in *C*. *P* values are calculated by unpaired two-tailed Student's *t* tests (*$P < 0.05$, **$P < 0.01$, ***$P < 0.001$, ****$P < 0.0001$).

endoplasmic-reticulum membranes (MAMs, Fig. 4*C*). IF with CALNEXIN as the ER marker s showed colocalization of BARD1, p53, and SERCA2 in the ER (Fig. 4*D*). Proximity Ligation Assay (PLA) on *BARD1*^{WT} and *BARD1*^{V523A} fibroblasts showed that BARD1–SERCA2, SERCA2–p53, and BARD1–p53 interacted in the ER/MAMs (Fig. 4*E*). We found no significant differences in the discrete fluorescent number of PLA dots per cell for the BARD1–SERCA2 interaction between *BARD1*^{WT} and *BARD1*^{V523A} fibroblasts (Fig. 4*F*), whereas the number of discrete fluorescent PLA dots per cell was significantly lower in *BARD1*^{V523A} fibroblasts compared to the *BARD1*^{WT} for the SERCA2–p53 and for the BARD1–p53 interactions (Fig. 4 *G* and *H*).

These data suggested that BARD1 might interact with both p53 and SERCA2 in the ER. To test this hypothesis, we performed a Co-IP from the ER fraction obtained by cellular fractionation of HEK293 cells -used because these experiments required a large number of cells that were not available from primary cells. BARD1, p53, and SERCA2 coimmunoprecipitated using an anti-BARD1 antibody (Fig. 5*A*). Reverse Co-IP using p53 (Fig. 5*B*) or anti-SERCA2 (Fig. 5*C*) antibodies supported that BARD1, p53, and SERCA2 coprecipitated. Same results were obtained by Co-IP in primary *BARD1*^{WT} and *BARD1*^{V523A} fibroblast cell lysates using an anti-BARD1 antibody (*SI Appendix*, Fig. S5*F*). These data suggested that BARD1 forms a trimer with p53 and SERCA2.

To validate this hypothesis, we performed Surface Plasmon Resonance (SPR) experiments using recombinantly expressed human proteins. First, we confirmed the binding of BARD1 to SERCA2, immobilized as ligand by noncovalent capture to an anti-his mAb coupled to the surface of a Biacore CM5 optical sensor chip. Recombinant BARD1 was passed over the immobilized SERCA2 ligand at 167 nM concentration in a single binding cycle (Fig. 5*D* and *SI Appendix*, Fig. S6*A*). To assess the strength of the BARD1–SERCA2 interaction we performed kinetic binding analysis of the BARD1–SERCA2 binding sensorgrams by mathematical curve fitting applying a Langmuir 1:1 binding model (Fig. 5*D* and *SI Appendix*, Fig. S6 *A* and *B*). Kinetic binding constants were determined from the fitted curves indicating that BARD1 strongly interacts with SERCA2 with a K_D of 6.0 ± 1.2 (Fig. 5*D* and *SI Appendix*, Fig. S6*B*). We further tested whether BARD1, SERCA2, and p53 could form a trimeric protein complex. By sequential injection BARD1 and p53 were passed at 167 nM concentration as analytes over the captured SERCA2 ligand (Fig. 5*E* and *SI Appendix*, Fig. S6*C*). A double-referenced sensorgram, generated by subtraction of an amine-activated flow cell 1 background reference curve and a

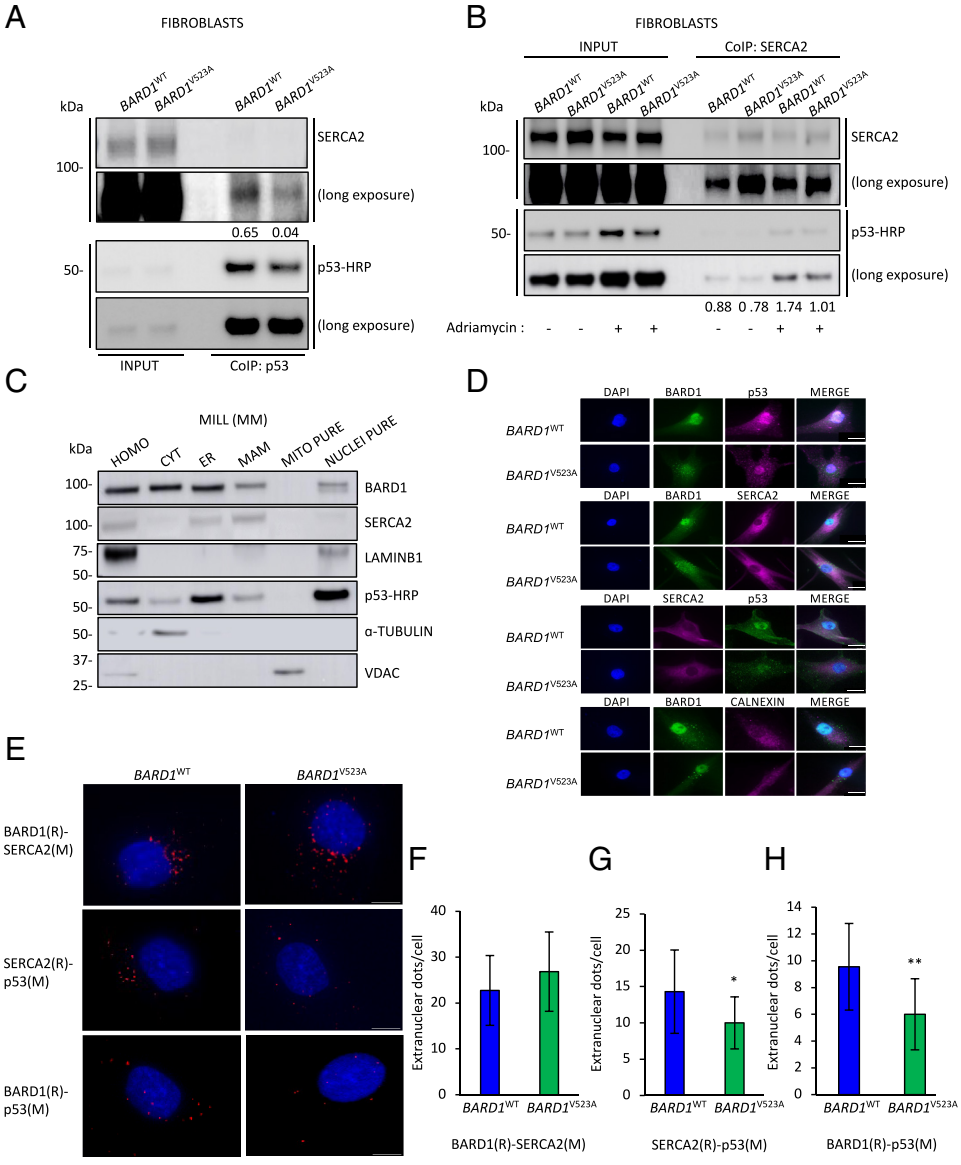

Fig. 4. BARD1 stabilizes p53–SERCA2 interaction. (*A*) Co-IP of endogenous SERCA2–p53 interaction using p53 antibody. Reduction of the coprecipitated p53–SERCA2 proteins was detected in *BARD1*^{V523A} cells compared to *BARD1*^{WT} cells. (*B*) Co-IP in *BARD1*^{WT} and *BARD1*^{V523A} fibroblasts showing reduced SERCA2–p53 interaction after Adriamycin (2 μM) treatment for 3 h using SERCA2 antibody as bait. (*C*) WB showing the amounts of BARD1 in the subcellular fractions of a mesothelioma cell line, Mill. HOMO: homogenate; CYT: cytosol; ER: endoplasmic reticulum; MAM: mitochondrial-associated membrane. MITO: mitochondria; Markers: mitochondria (VDAC), ER (SERCA2), nuclei (Lamin B1), cytosol (α-Tubulin). (*D*) IF: BARD1, SERCA2, p53 localization in *BARD1*^{WT} and *BARD1*^{V523A} fibroblasts. Cells were immunostained for BARD1, SERCA2, p53, and CALNEXIN (ER marker). BARD1, besides its nuclear localization, showed a diffuse pattern of punctate hyperfluorescent spots in the cytoplasm that colocalized with the ER, in both *BARD1*^{WT} and *BARD1*^{V523A} fibroblasts. Representative IF images from n = 10 fields of view. (Scale bars: 10 μm.) (*E*) PLA showing the interaction of BARD1–SERCA2, SERCA2–p53, and BARD1–p53 interactions (red dots) in the ER of *BARD1*^{WT} and *BARD1*^{V523A} fibroblasts (nuclei stained blue with DAPI). (Scale bars: 10 μm.) (*F–H*) Bar graph: Quantification of PLA red dots per cell showing reduced SERCA2–p53 (*G*) and reduced BARD1–p53 (*H*) interactions in *BARD1*^{V523A} fibroblasts *BARD1*^{WT}. No difference was found in the BARD1–SERCA2 interaction (*F*). Data shown are mean ± SD (n = 20 cells). Decimals: SERCA2/p53 in *A*; p53/SERCA2 in *B*. *P* values are calculated by unpaired two-tailed Student's *t* tests (**P* < 0.05, ***P* < 0.01).

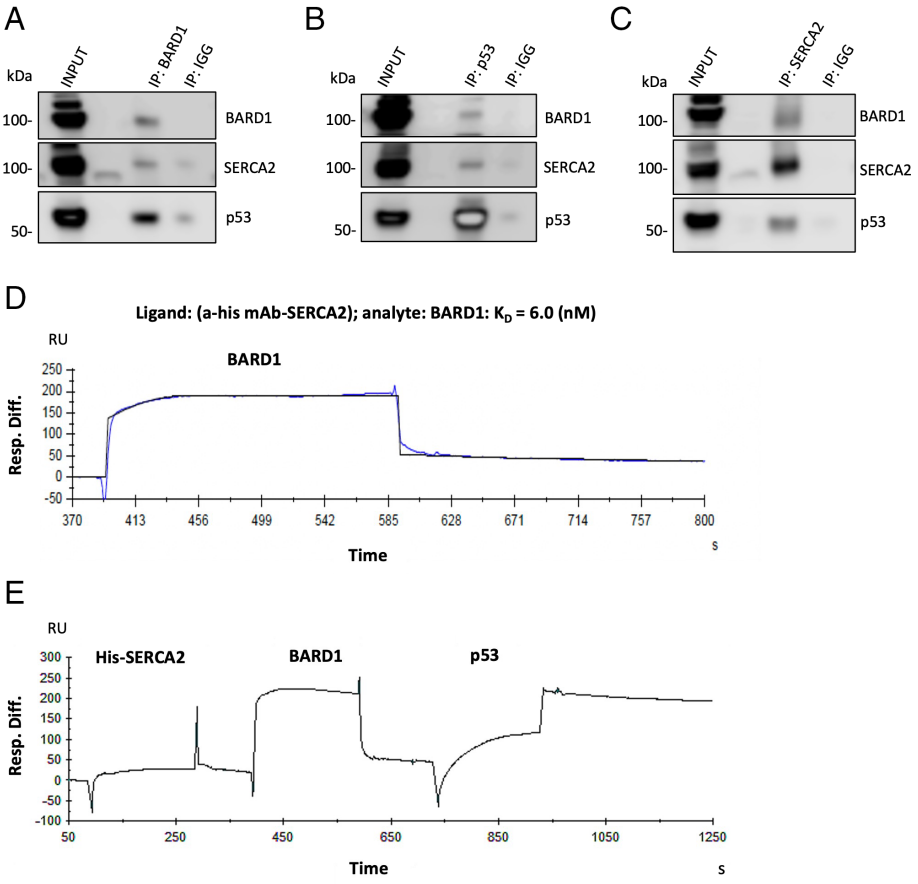

Fig. 5. BARD1, p53, and SERCA2 form a trimeric protein complex. (*A*–*C*) Co-IP of endogenous BARD1–SERCA2–p53 interaction using BARD1 (*A*), p53 (*B*), or SERCA2 (*C*) as bait in the ER fraction of HEK293A cells. (*D*) SPR sensorgram showing binding of BARD1167 nM passed as analyte over SERCA2 ligand, immobilized to the sensor chip surface by his-tag capturing. Kinetic constants and affinity were determined by sensorgram fitting using a Langmuir 1:1 fitting binding model. The fitted curve is shown. The calculated equilibrium dissociation constant (K_D = 6.0) is indicated. (*E*) His-tagged SERCA2 was captured as ligand on a Biacore sensor chip surface to which an anti-his mAb had covalently coupled. BARD1 and p53 were subsequently passed as analytes over the immobilized SERCA2 ligand at 167 nM concentration by sequential injection at a flow rate of 30 µL/min in Hepes Buffered Saline (HBS-EP) buffer. The shown curve represents a double-referenced sensorgram, obtained by subtraction of 1) an amine-activated reference flow cell (FC1) sensorgrams followed by 2) subtraction of a SERCA2 binding sensorgram generated without subsequent BARD1 and p53 injection in order to compensate for complex dissociation from the anti-his mAb during the sequential BARD1 and p53 analyte binding process. The shown curve was selected from experiments run in duplicate.

SERCA2 sensorgram run without subsequent BARD1 and p53 injection to compensate for complex dissociation from the anti-his mAb during the sequential analyte binding process, is shown in Fig. 5*E*. The sensorgrams show binding signals for both, BARD1 and p53, to his-tag captured SERCA2 ligand, thus confirming the formation of a trimolecular binding complex.

Reduced BARD1 Levels Favor Asbestos-Induced Transformation In Vitro and Biallelic *BARD1* Inactivation Is Detected in Invading Mesothelioma Cells. To test whether *BARD1* inactivation influences asbestos carcinogenesis, we performed in vitro foci transformation assays, exposing HM silenced for BARD1 to 5 µg/cm^2 of asbestos. Asbestos induced a significantly higher number of tridimensional foci in *BARD1*- silenced HM (Fig. 6 *A* and *B*). Proliferation assays revealed increased proliferation of *BARD1*^{V523A} fibroblasts compared with *BARD1*^{WT} upon exposure to IR (Fig. 6 *C*–*F*), and increased viability of *BARD1*^{V523A} fibroblasts exposed to H_2O_2 compared to the *BARD1*^{WT} counterpart (Fig. 6*G*).

IHC of *BARD1*^{V523A} mesothelioma biopsies revealed BARD1 and p53 staining in the superficial area containing benign atypical mesothelial hyperplasia. The positive staining of both BARD1 and p53 is evidence of at least one remaining functional *BARD1* allele capable of binding p53, preventing MDM2 binding and degradation of p53. The deeper part of the biopsy contains invading malignant mesothelioma cells, which for the most part show loss of both BARD1 and p53 staining, evidence of biallelic *BARD1* inactivation, with parallel loss of p53 likely due to its complete degradation (Fig. 6*H*). This interpretation was supported by gene expression analyses from the TCGA database showing a significant positive correlation between *BARD1* and *TP53* gene expression in 87 mesotheliomas (Fig. 6*I*). Together, these data support a pathogenic role of reduced *BARD1* levels, as observed in cells carrying the *BARD1*^{V523A} variants and in cells in which we down-regulated BARD1 using siRNAs, possibly in cooperation with asbestos, gene × environment interaction, in causing mesothelioma.

Germline *BARD1* Pathogenic Variants Are Associated with Mesothelioma. To investigate the frequency of germline *BARD1* mutations in mesotheliomas, regardless of age or evidence of asbestos exposure, we analyzed the germline DNA of 264 sporadic mesotheliomas for *BARD1* using WES, digital-MLPA, and Sanger sequencing. We tested 101 patients from the USA, 131 from Japan, and 32 from Italy. Survival information for these patients was not available. We found three carriers of rare *BARD1* mutations with a CADD score >20, all in the USA cohort (*SI Appendix*, Fig. S1 *B* and *C* and Table S3).

In addition to these three variants (*SI Appendix*, Table S3), we detected the variant p.Arg658Cys (CADD score of 24.3) in three US and two Japanese patients with sporadic mesothelioma and it was also detected in two cases in the initial screening in young patients. We did not include this variant among those we consider pathogenic because although its frequency in the western population is 0.0081, gnomAD v4 shows that this variant is frequent among Amish and Finnish people. Similarly, 9 Japanese mesothelioma patients carried the p.Ser241Cys. Although this mutation has a CADD score of 24.1 and is rare in the Western population (frequency = 0.00013), it has a frequency of 0.054 in the Japanese population. Because these variants are not rare in some populations, we are unsure about their possible pathogenic role and thus they were not included in *SI Appendix*, Table S3. Further studies would be needed to rule out a possible contributory role of these variants to mesothelioma, as some variants may be carcinogenic in specific contexts. For example, a study reported that two single germline *BARD1* mutations cause no obvious cellular phenotype, but when they exist simultaneously

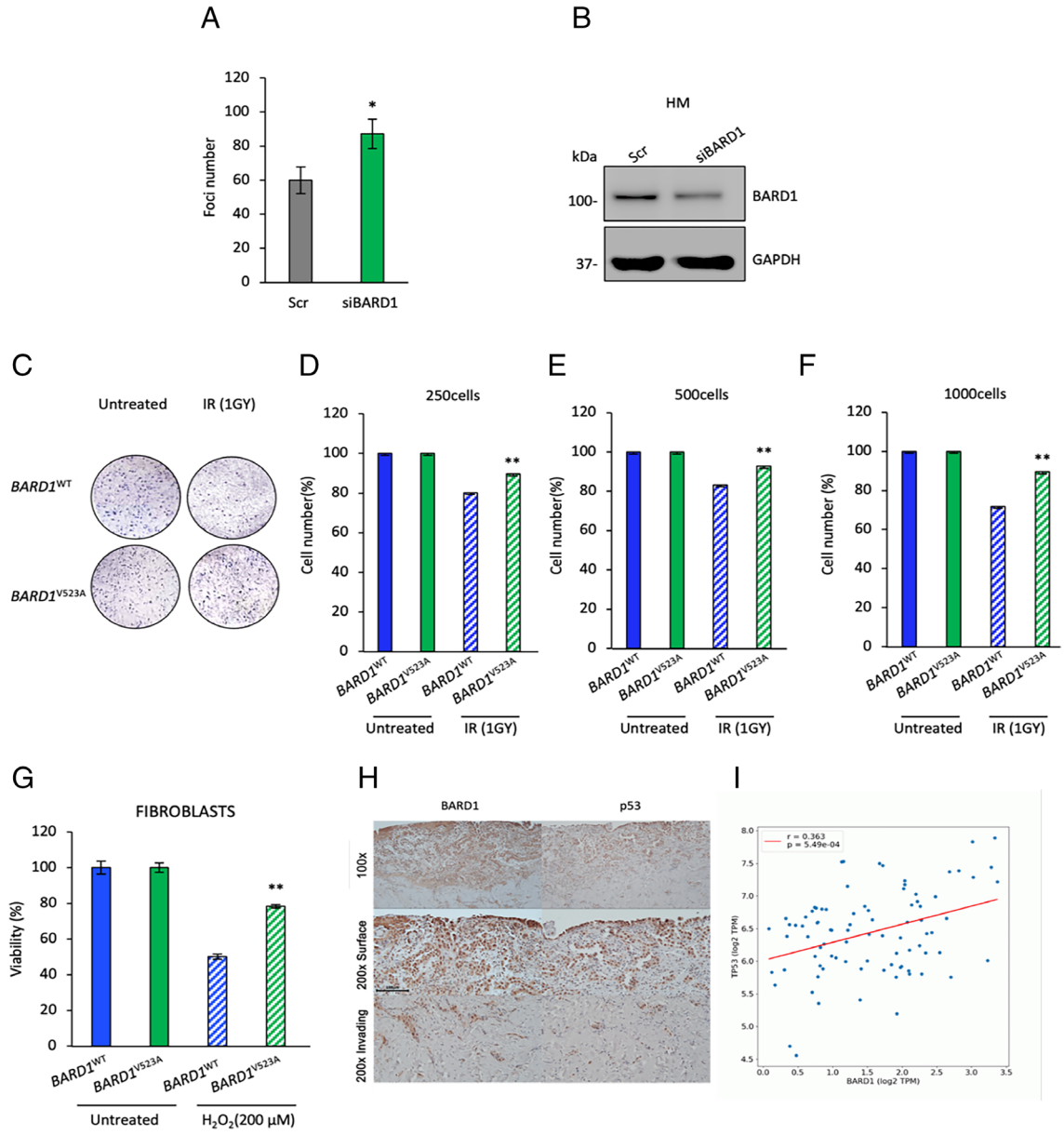

Fig. 6. BARD1 depletion and *BARD1*^{V523A} mutation induce malignant transformation. (*A* and *B*) In vitro transformation measured as tridimensional foci formation. Primary HM cells were silenced with scramble siRNA or a pool of siBARD1, and then exposed to crocidolite asbestos (5 µg/cm^2) in the presence of TNFα. Increased number of foci formation in *BARD1*-silenced HM. Data shown are mean ± SD of n = 3 technical replicates from n = 3 independent experiments. *P* values are calculated by unpaired two-tailed Student's *t* tests. (*$P < 0.05$). (*C–F*) Cell proliferation assay in *BARD1*^{WT} and *BARD1*^{V523A} fibroblasts after exposure to 1GY of IR. *BARD1*^{WT} and *BARD1*^{V523A} fibroblasts were seeded at 250 cells/well (*D*), 500 cells/well (*E*), and 1,000 cells/well (*F*) after exposure to 1GY of ionizing. Significantly higher cell proliferation was observed in *BARD1*^{V523A} fibroblasts. *P* values are calculated by unpaired two-tailed Student's *t* tests (**$P < 0.01$). (*G*) Cell viability assay in *BARD1*^{WT} and *BARD1*^{V523A} fibroblasts after treatment with 200 µM H_2O_2 for 3 h or left untreated. *BARD1*^{V523A} fibroblasts showed a significant increase in the percentage of viable cells after treatment with H_2O_2 compared with *BARD1*^{WT} cells. *P* values are calculated by unpaired two-tailed Student's *t* tests (**$P < 0.01$). (*H*) BARD1 and p53 immunostaining in mesothelioma tumor tissue sample from *BARD1*^{V523A} carrier (female). Photomicrograph at 100×, 200× Surface, and 200× Invading. (Scale bar: 100 µm.) (*I*) Scatter plot visualizing the correlation between *BARD1* and *TP53* gene expression in 87 cases of mesothelioma patients described in OncoDB (TCGA database).

in cis they promote tumorigenesis (32). Moreover, a mesothelioma patient with the *BARD1* variant p.Arg658Cys also had a pathogenic *BAP1* variant. The effect of *BARD1* variants in combination with other gene variants may be the subject of future studies.

Discussion

Recent studies revealed a larger than expected percentage of individuals carrying heterozygous germline variants (commonly called mutations) in various tumor suppressor genes: Depending on the gene involved the risk of cancer may be slightly increased or, at times, approach 100% (57). Genetically linked cancers develop for the most part in patients that are 10 to 30 y younger compared to their sporadic counterparts (2). Here, we have linked germline *BARD1* mutations to the development of mesothelioma in young patients. Therefore, *BARD1* should be included in the screening panel of mesothelioma patients for germline mutations. The carriers of the germline *BARD1* mutations studied here experienced a statistically significantly (*$P < 0.05$) improved survival compared to sporadic mesothelioma, with a median survival of 3.0 y, with 95% confidence limits (2.6, 23.0). This unlikely finding in sporadic mesothelioma is similar to mesotheliomas developing in carriers of germline *BAP1* mutations (8).

To investigate the significance of BARD1 inactivation, we studied the functional effects of one of these variants, *BARD1*^{V523A}, that we detected in the germline of a mesothelioma living patient

with the exceptional survival of 23 y, in spite of tumor cell invasion detected histologically (Fig. 1). We used the patient's primary *BARD1*^{V523A} heterozygous cells — that do not require any experimental manipulation — to investigate whether and how this *BARD1* mutation might influence key cellular signaling pathways. In parallel experiments, we validated the results in primary HM cells obtained from nonmalignant pleural effusions in which we down-regulated *BARD1* using siRNAs.

Studying the effects of both the *BARD1*^{V523A} variant and of reduced *BARD1* levels obtained using siRNAs in primary HM we found that: 1) *BARD1*^{V523A} impaired DNA repair and increased DNA damage; 2) *BARD1*^{V523A} as well as reduced BARD1 levels increase intracellular ROS production, an effect that contributes to DNA damage; 3) BARD1 modulates apoptosis through Ca^{2+} signaling and both *BARD1*^{V523A} as well as reduced BARD1 protein levels impair apoptosis because of decreased ER, cytosolic, and mitochondrial Ca^{2+} concentrations; 4) BARD1 modulates intracellular Ca^{2+} homeostasis in a TP53-dependent manner. Specifically, *BARD1*^{V523A} and downregulation of BARD1 leads to p53 degradation that in turn causes reduced TRPC6 activity and reduced p53–SERCA2 interaction resulting in reduced Ca^{2+} intracellular levels and decreased apoptosis; 5) BARD1 forms a trimeric complex with p53 and SERCA2 that colocalize in the ER and MAMs to modulate Ca^{2+} flux and apoptosis, which we demonstrated through Co-IP and SPR experiments; 6) *BARD1*^{V523A} as well as reduced BARD1 levels facilitate in vitro cell transformation by asbestos and ionizing irradiation (Fig. 7).

The similarity of the results in both, cells carrying *BARD1*^{V523A} heterozygous mutation and HM cells in which we down-regulated BARD1 using siRNAs, suggests that our results can be attributed to the reduced amounts of functional (wild-type allele) *BARD1* rather than to the specific mutation per se. Therefore, we anticipate that the deletion of *BARD1* 7-11 and the truncating deletion detected in the screening of sporadic mesotheliomas (*SI Appendix*, Tables S1 and S2) will induce similar alterations and therefore are pathogenic and contribute to mesothelioma in these patients. The literature supports that large deletions of *BARD1* predispose to breast and ovarian cancer (33). As for the remaining four missense *BARD1* mutations they are rare and their high CADD scores suggest that they are pathogenic. Functional studies were not conducted because cells from these patients were not available.

Our findings revealed that both *BAP1* and *BARD1* inactivate similar pathways: DNA repair, calcium signaling, and cell death, although through different mechanisms. These findings suggest that perturbations of these signaling pathways play a key role in the pathogenesis of mesothelioma. In addition, these findings suggest that mesotheliomas developing in *BAP1* and *BARD1*-mutant carriers may be susceptible to similar therapeutic approaches. Mesothelioma patients carrying *BAP1* mutations are more susceptible to Platinum and Pemetrexed chemotherapy (58); it seems possible that *BARD1*-mutant patients may also benefit from this therapy. Germline *BARD1* mutation carriers may also benefit from MDM2 inhibitors, such as XR-2, currently in clinical trial for prostate cancer (59). Moreover, recent results show that *BARD1* loss increased sensitivity to the PARP inhibitors Olaparib and Rucaparib across a panel of prostate cancer cell lines (60), suggesting a potential antitumor activity in patients with *BARD1* mutations.

In the past century mesothelioma was characteristically a disease of older men who had worked in the asbestos industry (2). Mesotheliomas in patients younger than 55 y old, and in women, were rare (2). The question is why are we increasingly seeing mesotheliomas in young patients, often women, who have not worked in the asbestos industry? In recent studies, we found that about 50% of mesothelioma patients younger than 55 with no evidence of professional asbestos exposure carried germline *BAP1* mutations – and occasionally pathogenic mutations of *TP53*, *BLM*, *BRCA1,* and *BRCA2*, etc. These findings have been independently supported (14–16, 61). Here, we report that about 1.8% of all mesothelioma patients and 4.9% of those younger than 55, carried rare germline variants of the *BARD1* gene that our computational analyses, CADD score >20, and in vitro mechanistic studies found pathogenic. Together, these findings indicate that mesotheliomas in young patients are often caused by germline mutations of tumor suppressor genes.

It is very important that those caring for these patients understand that genetically linked mesotheliomas, especially when detected at an early stage, have a much less aggressive clinical course compared to patients with asbestos-induced mesotheliomas: These are different diseases. The former is minimally invasive, patients survive for several years and respond to therapy. Some patients have been cured, like the patient carrying germline *BARD1*^{V523A} who donated her cells for this study. However, they are at risk of developing additional cancers, therefore they require screening for early

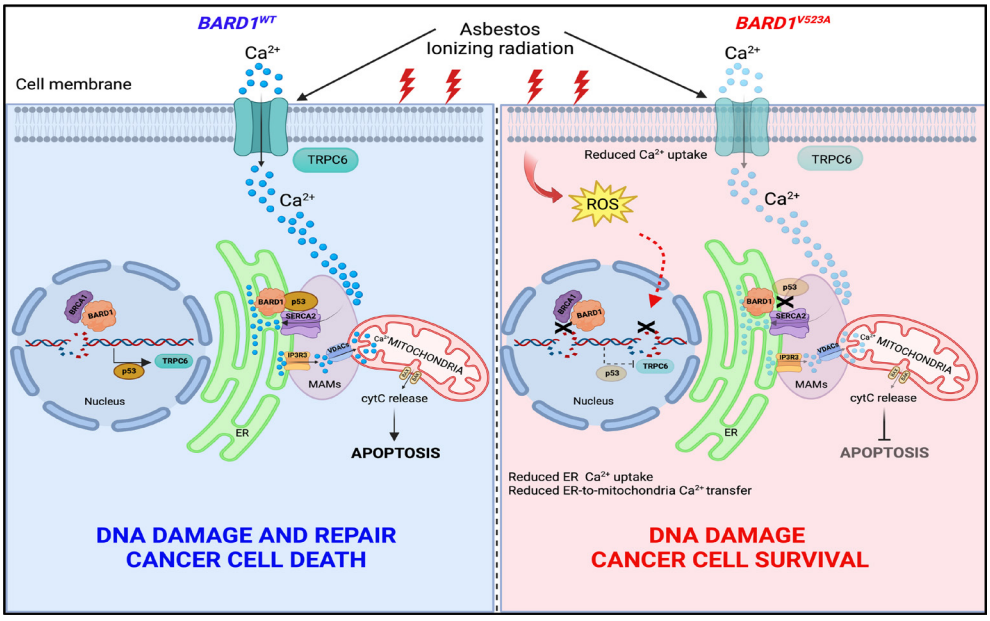

Fig. 7. Carriers of *BARD1*^{V523A} mutation have impaired DNA repair and apoptosis, promoting malignant cell transformation. Schematic representation showing how BARD1 regulates DNA damage response and cell death. In *BARD1*^{WT} individuals, nuclear BARD1 regulates DNA repair through BRCA1 binding upon DNA damage; In parallel, BARD1 regulates apoptosis by a p53-dependent induction of TRPC6 expression and by forming a trimeric complex with SERCA2 and p53 in the ER of the cell, thus modulating intracellular Ca^{2+} flux and cell death. In *BARD1*^{V523A}, reduced BARD1 activity results in increased DNA damage, increased ROS production, reduced TRPC6 expression, and loss of BARD1–SERCA2–p53 trimeric complex in the ER, resulting in impaired Ca^{2+} flux and resistance to apoptosis.

cancer detection that can be life-saving (8, 13, 17). Instead, sporadic mesotheliomas, often asbestos-induced, are highly invasive malignancies resistant to therapy and these patients have a dismal median survival of 12 mo from diagnosis (2).

Our results present the paradox that on one hand, *BARD1* mutations cause mesothelioma, and on the other hand, mesotheliomas in *BARD1*$^{+/-}$ carriers are significantly less aggressive and minimally invasive. Why? Either their tumor cells are less aggressive, or *BARD1*$^{+/-}$ carriers can "fight" mesothelioma growth, or both. Remarkably, we see the same paradox in germline *BAP1*$^{+/-}$ carriers.

Younger age does not appear to play a major role, since asbestos and erionite-related mesothelioma in those exposed since birth age, are as aggressive as those developing in older patients. Similarly, inactivation of *BAP1* and *BARD1* in cancer cells may not be the only factor, as asbestos-related mesotheliomas with acquired *BAP1* or *BARD1* mutations have an improved survival that is measured in months, not in years (2, 8, 11, 58) and Fig. 1*A*. Therefore, in addition of the effects on the tumor cells, it seems possible that reduced *BAP1* and *BARD1* levels may induce epigenetic changes and/or influence signal pathways in the tumor microenvironment (TME), resulting in an altered TME/immune response that impair cancer growth.

In summary, we uncovered common signaling pathways affected by reduced BAP1 and BARD1 levels that lead to the development of mesothelioma in young adults. We hope that by studying these pathways we will identify those responsible for the improved survival and that by targeting these same pathways in patients with sporadic mesothelioma, and possibly with other malignancies, we will improve their survival too. The NCI has now opened two clinical trials in the Bethesda Medical Center to study mesothelioma in carriers of pathogenic germline mutations and in their family members who inherited the same mutation, directed by Drs. Hassan (natural history protocol NCT03830229) and Schrump (surgical surveillance protocol NCT04431024). These trials are helping us to identify the most effective preventive, early detection and therapeutic approaches for these patients. Therefore, for the 8 to 16% growing fraction of mesotheliomas developing in carriers of germline mutations, there is reason for optimism.

Materials and Methods

Subjects. *BARD1* mutated carriers and their wild-type counterparts provided informed written consent. The collection and use of patient information and samples were approved by the Institutional Review Board (IRB) of the University of Hawaii (IRB no. CHS14406).

Study Population, Exome Sequencing, Digital-MLPA Analysis, Validation of Candidate Variants, Sanger Sequencing, Gene-Level Analysis. See *SI Appendix*.

Cell Cultures, Reagents, Gene Silencing with siRNA, Adenoviruses, Antibodies. According to standard procedures; see *SI Appendix*.

Immunoblotting, Quantitative PCR, Co-IP, IF, Duolink Proximity Ligation In Situ Assay, In Vitro Cell Transformation Assay, IHC. According to standard procedures; see *SI Appendix*.

Subcellular Fractionation, Kinetics of H2AX Phosphorylation. Performed as described (48). See *SI Appendix* for additional details.

Determination of Micronuclei Frequency. It was performed as described (62). Micronuclei from a minimum of 100 interphase cells were quantified in crocidolite-treated or IR-treated cultures, as well as in untreated (PBS only) cultures, from two independent experiments (biological replicates: n = 2 *BARD1*^{WT}; n = 2 *BARD1*^{V523A}). See *SI Appendix* for additional details.

Intracellular Ca^{2+} Concentration Measurements. This was performed as described (48). See *SI Appendix* for details.

SPR Experiments. This was performed as described (63). See *SI Appendix* for details.

Statistics and Reproducibility. *P* values were calculated using a two-tailed unpaired Student *t* test, unless otherwise specified. *P* values < 0.05 were considered statistically significant and marked with asterisks (*$P < 0.05$; **$P < 0.01$; ***$P < 0.001$; ****$P < 0.0001$), as indicated in the figure legends. All data collected met the normal distribution assumption of the test. Data are represented as mean ± SD, unless otherwise specified in the figure legends. The exact sample size (n) for experimental groups/conditions and whether samples represent technical, or cell culture replicates are indicated in the figure legends. The results shown are representative of experiments independently conducted three times that produced similar results.

Data, Materials, and Software Availability. All data are included in the manuscript and *SI Appendix*.

ACKNOWLEDGMENTS. We are grateful to the patient who donated her specimens for research. We would like to acknowledge Christine Farrar (the University of Hawaii Cancer Center Microscopy core facility) and Alexandra Gurary (Molecular & Cellular Immunology core of the University of Hawai'i John A. Burns School of Medicine) for their technical assistance; This work utilized a Leica Thunder three dimensional (3D) Live Cell Imaging System that was purchased with funding from a NIH Shared Instrumentation Grant 1S10ODO28515-01. H.Y. and M.C. report funding from the National Institute of Environmental Health Sciences 1R01ES030948-01 (H.Y. and M.C.), the National Cancer Institute (NCI) R01CA2372351 and R01CA237235-01A1 (H.Y.M.C.) and 1R01CA198138 (M.C.), the US Department of Defense W81XWH-16-1-0440 (H.I.P., H.Y., and M.C.), and from the UH Foundation through donations from: Barry and Virginia Weinman; the Riviera United-4-a Cure (H.Y. and M.C.), the Melohn Family Endowment, the Honeywell International Inc., Richard L. and Susan Fried; Turbin Chu Family Fundthe Germaine Hope Brennan Foundation, and the Maurice and Joanna Sullivan Family Foundation (M.C.). H.I.P. and H.Y. report funding from the Early Detection Research Network NCI 5U01CA214195-04. H.I.P. reports funding from Genentech, Belluck and Fox LLP. C.G. and P.P. report funding from the Italian Association for Cancer Research (IG-23670 to P.P. and IG-19803 to C.G.), AROSE, Progetti di Rilevante Interesse Nazionale (PRIN2017E5L5P3 to P.P. and PRIN20177E9EPY to C.G.), the Italian Ministry of Health (GR-2013-02356747 to C.G.), the European Research Council (853057-InflaPML to C.G.), and the University of Ferrara. J.N.O. is a CPRIT Scholar in Cancer Research sponsored by the Cancer Prevention and Research Institute of Texas. Work at the Center for Theoretical Biological Physics was sponsored by the NSF (Grant PHY-2019745 and PHY-2210291), and by the Welch Foundation (Grant C-1792).

Author affiliations: [a]Thoracic Oncology, University of Hawaii Cancer Center, Honolulu, HI 96816; [b]Department of Genetics, School of Medicine, Hyogo Medical University, Hyogo 663-8501, Japan; [c]Department of Medical Sciences, Laboratory for Technologies of Advanced Therapies, University of Ferrara, Ferrara 44121, Italy; [d]NBS-C Bioscience & Consulting GmbH, Vienna 1230, Austria; [e]Shanghai Institute for Advanced Immunochemical Studies, Shanghai Tech University, Shanghai 201210, China; [f]Center for Theoretical Biological Physics, Rice University, Houston, TX 77005; [g]Department of Molecular Biosciences and Bioengineering, University of Hawaii at Manoa, Honolulu, HI 96822; [h]Desert Research Institute, Reno, NV 89512; [i]Mesothelioma Unit, Azienda Ospedaliera Santo Antonio and Santo Biagio (SS) Antonio e Biagio e Cesare Arrigo, Alessandria 15121, Italy; [j]Thoracic Surgery Branch, Center for Cancer Research, National Cancer Institute, Bethesda, MD 20892-1201; [k]Department of Cardiothoracic Surgery, New York University, New York, NY 10016; [l]Department of Oncogenetics, MRC Holland, Amsterdam 1057, the Netherlands; [m]Department of Dermatology, Stanford University Medical Center, Stanford, CA 94305; and [n]Division of Immunology, Department of Medical Biochemistry and Biophysics, Karolinska Institutet, Stockholm 17165, Sweden

1. J. Zhao, The global trends in incidence, death, burden and risk factors of early-onset cancer from 1990 to 2019. *BMJ Oncol.* **2**, 12 (2023).
2. M. Carbone *et al.*, Mesothelioma: Scientific clues for prevention, diagnosis, and therapy. *CA Cancer J. Clin.* **69**, 402–429 (2019).
3. M. Carbone, H. Yang, H. I. Pass, E. Taioli, Did the Ban on asbestos reduce the incidence of mesothelioma? *J. Thorac. Oncol.* **18**, 694–697 (2023).
4. I. Roushdy-Hammady, J. Siegel, S. Emri, J. R. Testa, M. Carbone, Genetic-susceptibility factor and malignant mesothelioma in the Cappadocian region of Turkey. *Lancet* **357**, 444–445 (2001).

5. M. Carbone *et al.*, A mesothelioma epidemic in Cappadocia: Scientific developments and unexpected social outcomes. *Nat. Rev. Cancer* **7**, 147–154 (2007).
6. J. R. Testa *et al.*, Germline BAP1 mutations predispose to malignant mesothelioma. *Nat. Genet.* **43**, 1022–1025 (2011).
7. M. Carbone *et al.*, BAP1 and cancer. *Nat. Rev. Cancer* **13**, 153–159 (2013).
8. M. Carbone *et al.*, Medical and surgical care of patients with mesothelioma and their relatives carrying germline BAP1 mutations. *J. Thorac. Oncol.* **17**, 873–889 (2022).
9. M. Carbone *et al.*, Biological mechanisms and clinical significance of BAP1 mutations in human cancer. *Cancer Discov.* **10**, 1103–1120 (2020).
10. F. Baumann *et al.*, Mesothelioma patients with germline BAP1 mutations have 7-fold improved long-term survival. *Carcinogenesis* **36**, 76–81 (2015).
11. S. Pastorino *et al.*, A subset of mesotheliomas with improved survival occurring in carriers of BAP1 and other germline mutations. *J. Clin. Oncol.* **36**, 3485–3494 (2018).
12. R. Hassan *et al.*, Inherited predisposition to malignant mesothelioma and overall survival following platinum chemotherapy. *Proc. Natl. Acad. Sci. U.S.A.* **116**, 9008–9013 (2019).
13. M. Kittaneh, C. Berkelhammer, Detecting germline BAP1 mutations in patients with peritoneal mesothelioma: Benefits to patient and family members. *J. Transl. Med.* **16**, 194 (2018).
14. M. Sculco *et al.*, Malignant pleural mesothelioma: Germline variants in DNA repair genes may steer tailored treatments. *Eur. J. Cancer* **163**, 44–54 (2022).
15. V. Panou, O. D. Roe, Inherited genetic mutations and polymorphisms in malignant mesothelioma: A comprehensive review. *Int. J. Mol. Sci.* **21**, 4327 (2020).
16. O. D. Mitchell *et al.*, Germline variants incidentally detected via tumor-only genomic profiling of patients with mesothelioma. *JAMA Netw. Open* **6**, e2327351 (2023).
17. Z. I. Hu *et al.*, Meningiomas in patients with malignant pleural mesothelioma harboring germline BAP1 mutations. *J. Thorac. Oncol.* **17**, 461–466 (2022).
18. M. Carbone, M. Minaai, Y. Takinishi, I. Pagano, H. Yang, Preventive and therapeutic opportunities: Targeting BAP1 and/or HMGB1 pathways to diminish the burden of mesothelioma. *J. Transl. Med.* **21**, 749 (2023).
19. D. E. Jensen *et al.*, BAP1: A novel ubiquitin hydrolase which binds to the BRCA1 RING finger and enhances BRCA1-mediated cell growth suppression. *Oncogene* **16**, 1097–1112 (1998).
20. H. Nishikawa *et al.*, BRCA1-associated protein 1 interferes with BRCA1/BARD1 RING heterodimer activity. *Cancer Res.* **69**, 111–119 (2009).
21. U. K. Westermark *et al.*, BARD1 participates with BRCA1 in homology-directed repair of chromosome breaks. *Mol. Cell Biol.* **23**, 7926–7936 (2003).
22. J. M. Stark, A. J. Pierce, J. Oh, A. Pastink, M. Jasin, Genetic steps of mammalian homologous repair with distinct mutagenic consequences. *Mol. Cell Biol.* **24**, 9305–9316 (2004).
23. W. Zhao *et al.*, BRCA1-BARD1 promotes RAD51-mediated homologous DNA pairing. *Nature* **550**, 360–365 (2017).
24. R. Honda, H. Tanaka, H. Yasuda, Oncoprotein MDM2 is a ubiquitin ligase E3 for tumor suppressor p53. *FEBS Lett.* **420**, 25–27 (1997).
25. I. Irminger-Finger *et al.*, Identification of BARD1 as mediator between proapoptotic stress and p53-dependent apoptosis. *Mol. Cell* **8**, 1255–1266 (2001).
26. A. Feki *et al.*, BARD1 induces apoptosis by catalysing phosphorylation of p53 by DNA-damage response kinase. *Oncogene* **24**, 3726–3736 (2005).
27. K. Tsukada *et al.*, BLM and BRCA1-BARD1 coordinate complementary mechanisms of joint DNA molecule resolution. *Mol. Cell* **84**, 640–658.e10 (2024).
28. M. Capasso *et al.*, Common variations in BARD1 influence susceptibility to high-risk neuroblastoma. *Nat. Genet.* **41**, 718–723 (2009).
29. B. M. Norquist *et al.*, Inherited mutations in women with ovarian carcinoma. *JAMA Oncol.* **2**, 482–490 (2016).
30. C. Ghimenti *et al.*, Germline mutations of the BRCA1-associated ring domain (BARD1) gene in breast and breast/ovarian families negative for BRCA1 and BRCA2 alterations. *Genes Chromosomes Cancer* **33**, 235–242 (2002).
31. M. Suszynska, P. Kozlowski, Summary of BARD1 mutations and precise estimation of breast and ovarian cancer risks associated with the mutations. *Genes (Basel)* **11**, 798 (2020).
32. W. Li *et al.*, A synergetic effect of BARD1 mutations on tumorigenesis. *Nat. Commun.* **12**, 1243 (2021).
33. Y. M. Hawsawi *et al.*, BARD1 mystery: Tumor suppressors are cancer susceptibility genes. *BMC Cancer* **22**, 599 (2022).
34. K. Agiannitopoulos *et al.*, Copy number variations (CNVs) account for 10.8% of pathogenic variants in patients referred for hereditary cancer testing. *Cancer Genomics Proteomics.* **20**, 448–455 (2023).
35. A. Benard-Slagter *et al.*, Digital multiplex ligation-dependent probe amplification for detection of key copy number alterations in T- and B-cell lymphoblastic leukemia. *J. Mol. Diagn.* **19**, 659–672 (2017).
36. P. Rentzsch, D. Witten, G. M. Cooper, J. Shendure, M. Kircher, CADD: Predicting the deleteriousness of variants throughout the human genome. *Nucleic Acids Res.* **47**, D886–D894 (2019).
37. S. Gudmundsson *et al.*, Variant interpretation using population databases: Lessons from gnomAD. *Hum. Mutat.* **43**, 1012–1030 (2022).
38. Y. Itan *et al.*, The mutation significance cutoff: Gene-level thresholds for variant predictions. *Nat. Methods* **13**, 109–110 (2016).
39. Y. Yoshikawa, M. Emi, T. Nakano, G. Gaudino, Mesothelioma developing in carriers of inherited genetic mutations. *Transl. Lung Cancer Res.* **9**, S67–S76 (2020).
40. M. Kircher *et al.*, A general framework for estimating the relative pathogenicity of human genetic variants. *Nat. Genet.* **46**, 310–315 (2014).
41. D. B. Chapel, J. J. Schulte, A. N. Husain, T. Krausz, Application of immunohistochemistry in diagnosis and management of malignant mesothelioma. *Transl. Lung Cancer Res.* **9**, S3–S27 (2020).
42. A. J. McCambridge *et al.*, Progress in the management of malignant pleural mesothelioma in 2017. *J. Thorac. Oncol.* **13**, 606–623 (2018).
43. D. A. Altomare *et al.*, Losses of both products of the Cdkn2a/Arf locus contribute to asbestos-induced mesothelioma development and cooperate to accelerate tumorigenesis. *PLoS One* **6**, e18828 (2011).
44. M. Nasu *et al.*, High incidence of somatic BAP1 alterations in sporadic malignant mesothelioma. *J. Thorac. Oncol.* **10**, 565–576 (2015).
45. S. Richards *et al.*, Standards and guidelines for the interpretation of sequence variants: A joint consensus recommendation of the American College of Medical Genetics and Genomics and the Association for Molecular Pathology. *Genet. Med.* **17**, 405–424 (2015).
46. K. S. Raraigh *et al.*, Functional assays are essential for interpretation of missense variants associated with variable expressivity. *Am. J. Hum. Genet.* **102**, 1062–1077 (2018).
47. A. I. Adamovich *et al.*, Functional analysis of BARD1 missense variants in homology-directed repair and damage sensitivity. *PLoS Genet.* **15**, e1008049 (2019).
48. A. Bononi *et al.*, BAP1 regulates IP3R3-mediated Ca2+ flux to mitochondria suppressing cell transformation. *Nature* **546**, 549–553 (2017).
49. A. Xu, L. J. Wu, R. M. Santella, T. K. Hei, Role of oxyradicals in mutagenicity and DNA damage induced by crocidolite asbestos in mammalian cells. *Cancer Res.* **59**, 5922–5926 (1999).
50. E. P. Rogakou, C. Boon, C. Redon, W. M. Bonner, Megabase chromatin domains involved in DNA double-strand breaks in vivo. *J. Cell Biol.* **146**, 905–916 (1999).
51. U. S. Srinivas, B. W. Q. Tan, B. A. Vellayappan, A. D. Jeyasekharan, ROS and the DNA damage response in cancer. *Redox Biol.* **25**, 101084 (2019).
52. V. Tembe *et al.*, The BARD1 BRCT domain contributes to p53 binding, cytoplasmic and mitochondrial localization, and apoptotic function. *Cell Signal* **27**, 1763–1771 (2015).
53. M. Bonora *et al.*, Subcellular calcium measurements in mammalian cells using jellyfish photoprotein aequorin-based probes. *Nat. Protoc.* **8**, 2105–2118 (2013).
54. E. Madan, R. Gogna, B. Keppler, U. Pati, p53 increases intra-cellular calcium release by transcriptional regulation of calcium channel TRPC6 in GaQ3-treated cancer cells. *PloS One* **8**, e71016 (2013).
55. C. Giorgi *et al.*, p53 at the endoplasmic reticulum regulates apoptosis in a Ca2+-dependent manner. *Proc. Natl. Acad. Sci. U.S.A.* **112**, 1779–1784 (2015).
56. C. Giorgi, S. Marchi, P. Pinton, The machineries, regulation and cellular functions of mitochondrial calcium. *Nat. Rev. Mol. Cell Biol.* **19**, 713–730 (2018).
57. M. Carbone *et al.*, Tumour predisposition and cancer syndromes as models to study gene-environment interactions. *Nat. Rev. Cancer* **20**, 533–549 (2020), 10.1038/s41568-020-0265-y.
58. A. Louw *et al.*, BAP1 loss by immunohistochemistry predicts improved survival to first-line platinum and pemetrexed chemotherapy for patients with pleural mesothelioma: A validation study. *J. Thorac. Oncol.* **17**, 921–930 (2022).
59. M. Wu *et al.*, Novel MDM2 inhibitor XR-2 exerts potent anti-tumor efficacy and overcomes enzalutamide resistance in prostate cancer. *Front. Pharmacol.* **13**, 871259 (2022).
60. K. M. Dillon *et al.*, PALB2 or BARD1 loss confers homologous recombination deficiency and PARP inhibitor sensitivity in prostate cancer. *NPJ Precis Oncol.* **6**, 49 (2022).
61. V. Panou *et al.*, Frequency of germline mutations in cancer susceptibility genes in malignant mesothelioma. *J. Clin. Oncol.* **36**, 2863–2871 (2018).
62. A. Bononi *et al.*, Heterozygous germline BLM mutations increase susceptibility to asbestos and mesothelioma. *Proc. Natl. Acad. Sci. U.S.A.* **117**, 33466–33473 (2020).
63. F. Novelli *et al.*, BAP1 forms a trimer with HMGB1 and HDAC1 that modulates gene x environment interaction with asbestos. *Proc. Natl. Acad. Sci. U.S.A.* **118**, e2111946118 (2021).